^{101}Tc produced by the (^{3}He,$pn\gamma$) reaction

D. G. Savage,* Hurol Aslan,† Ben Crowe,‡ Tim Dague, Sadek Zeghib,§ F. A. Rickey, and P. C. Simms
Tandem Accelerator Laboratory, Department of Physics, Purdue University, Lafayette, Indiana 47907
(Received 18 June 1996)

The nuclear structure of ^{101}Tc was studied using the ^{100}Mo(^{3}He,$pn\gamma$) reaction, which has populated most states in the nucleus below 2 MeV excitation energy. The proton exit channel was isolated from competing reaction channels by operating γ-ray detectors in coincidence with a large-solid-angle proton detector. The experiments included γ-ray excitation functions, γ-ray angular distributions, and γ-γ coincidences. The results were interpreted using a particle-rotor model. [S0556-2813(97)03501-2]

PACS number(s): 25.55.Hp, 27.60.+j, 23.20.Lv

I. INTRODUCTION

The use of the spherical shell model to interpret the structure of closed-shell nuclei is generally accepted. Far from closed shells (particularly in the rare-earth and actinide regions) nuclei exhibit regular rotational bands accepted as evidence for large permanent deformations. Between these extremes lie the so-called transitional nuclei. It seems probable that deformations must exist in transitional nuclei, but the questions of where they exist, and their magnitudes, are intriguing. The traditional view has been that vibrations about spherical shapes are the dominant collective degree of freedom near closed shells, and that collective rotations do not set in until there are many nucleons outside the closed shell. But the recognition of rotational features can be obscured because the Coriolis interaction, which is an integral part of rotational models, can distort the familiar patterns of rotational bands. In fact vibrational models and rotational models can provide similar interpretations of states near the yrast line in transitional nuclei. Hence heavy-ion reactions, which preferentially populate yrast states, do not distinguish between these models. On the other hand, we have found [1,2] that most states in a nucleus below 2 MeV excitation can be observed using ^{3}He fusion reactions with projectile energy a few MeV above the Coulomb barrier. This paper reports our investigation of ^{101}Tc, in which we have approximately doubled the known states below 2 MeV.

Since ^{101}Tc has 58 neutrons, it might be expected to be deformed, and in fact our data show evidence for several rotational bands. Accordingly, we have used a symmetric-rotor model for our interpretation of the data. The model utilizes a rotational Hamiltonian in the strong coupling limit modified to include a variable moment of inertia [3]. Pairing is treated by the BCS formalism. The Coriolis and recoil terms are treated to all order. This basic model has been used for years to interpret strongly deformed nuclei.

The ^{100}Mo(^{3}He,$pn\gamma$)^{101}Tc reaction was used in this experiment. A large-solid-angle proton detector was operated in coincidence with γ-ray detectors to separate the pn exit channel from xn and αxn channels. The improvement in the data was striking, which permitted us to see many weak γ-ray transitions that would have been lost without the proton gate.

The measurements include γ-ray excitation functions, angular distributions, and γ-γ coincidences. The degree of nuclear orientation observed in these experiments is lower than that obtained with heavy-ion reactions, hence spin assignments based on angular distributions can be less definite. However, the γ-ray excitation function can be used with the angular distribution to make spin assignments, as will be discussed later. Measurements for many weak γ rays were distorted by other γ rays with similar energy. This problem was minimized by using directional correlations in the coincidence data to make spin assignments.

II. EXPERIMENTAL TECHNIQUES

The target was a foil of isotopically enriched ^{100}Mo rolled to a uniform thickness of 2.1 mg/cm^{2}. The composition was 97.4% ^{100}Mo, 0.96% ^{98}Mo, and less than 0.5% impurities of ^{92,94,95,96,97}Mo. The ^{3}He beam currents of 10–25 nA were supplied by the Purdue FN Tandem Van de Graaff accelerator.

Data was collected on a DEC Micro Vax 3400 computer through a CAMAC interface. The proton detectors were thin plastic scintillators with a total solid angle of 66%. The two hyper-pure Ge γ-ray detectors used had energy resolutions of $\sim$ 2.0 keV at 1332 keV and efficiencies of $\sim$ 20%. Two techniques were used to facilitate high γ-ray counting rates. The ^{3}He beam was electrostatically deflected off the target as soon as a γ ray was detected to minimize the probability of pileup from subsequent γ rays. The beam was held off the target until the accepted event was processed. ORTEC 673 spectroscopy amplifiers were used with the γ-ray detectors. These instruments include a gated integrator, in addition to the usual active filter, to improve the signal-to-noise ratio. The addition of the gated integrator reduced the amplifier pulse width by 60% with negligible loss in γ-ray energy

*Present address: Department of Physics, Hampton University, Hampton, VA 23668.
†Present address: Department of Nuclear Engineering, Hacettepe University, Ankara, Turkey.
‡Present address: Triangle Universities Nuclear Laboratory, Durham, NC 27706.
§Present address: Institut des Sciences Exactes et Technologie, Universite de Constantine, Constantine, Algeria.

 © 1997 The American Physical Society

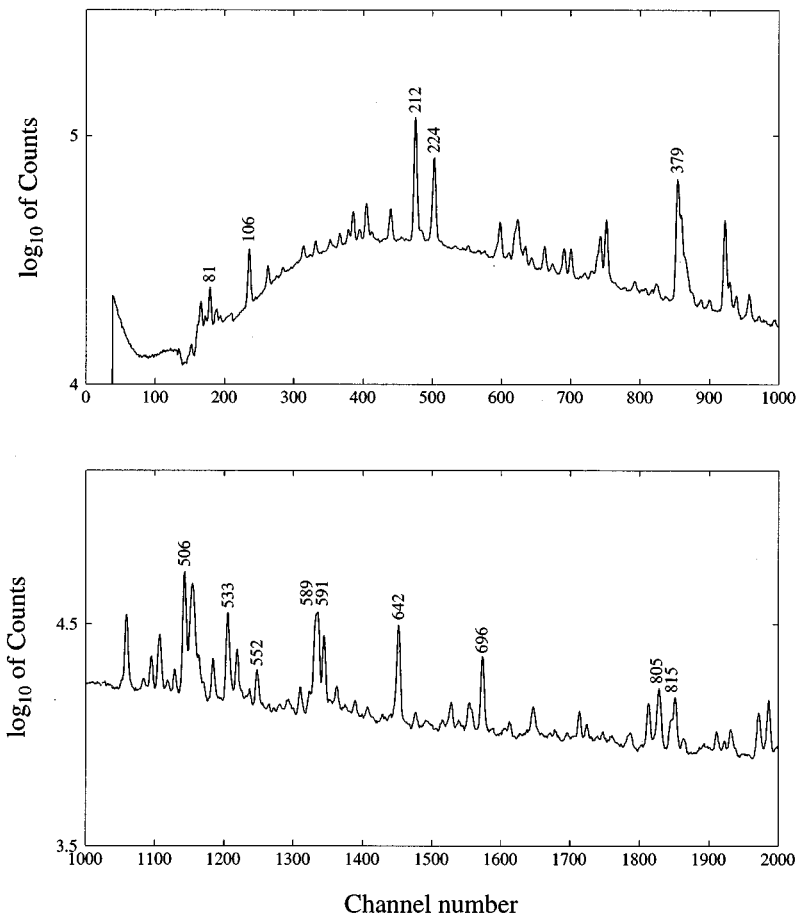

FIG. 1. A portion of a proton-gated singles spectrum from the ^{100}Mo(^{3}He,$pn\gamma$)^{101}Tc reaction at a laboratory energy of 16.5 MeV.

resolution. These techniques permit efficient data collection with average γ-ray counting rates of approximately 100 000 per second.

Time-to-amplitude converters (TAC) were used in the coincidence system. The TAC was started by the γ-ray detector and stopped by the proton detector. Two TAC's were required for the proton$-\gamma$-γ coincidence system. A separate digital logic circuit insured that the same proton pulse stopped both TAC's. The TAC spectra were processed in the on-line computer so that flexible windows could be used to define true and chance coincidences. The chance coincidence counting rate is proportional to the product of the window width times the singles-counting rate. Since the singles rate is large, it is necessary to minimize the window width to obtain a satisfactory true-to-chance coincidence ratio. The time jitter of the pulse from the γ-ray detector system is inversely proportional to the energy of the γ ray. Therefore, the window widths were adjusted as a function of the γ-ray energy for each coincidence event to increase the true-to-chance ratio. The true and chance windows always had the same width. Chance coincidences were subtracted as the data was accumulated. The window width varied from about 70 nsec for 50 keV γ rays to 10 nsec for γ rays with energy above 500 keV.

The time jitter for low-energy γ rays is so large that many of them are lost in a coincidence experiment. Elron STD-N-1 snap-off triggers were used for the γ-ray timing signals. The coincidence efficiency was approximately 35% for an 80 keV γ ray. The efficiency increases to 100% for γ-ray energies above 200 keV.

The chance coincidence spectrum from a start-stop TAC has an exponential shape because more than one stop pulse can occur within the range of the TAC. This effect would cause a 9% error in chance coincidence subtraction at the high counting rates used in these experiments. The effect was removed by introducing a fixed dead time in the stop input of the TAC. Additional experimental information is given in Ref. [4].

A. Excitation functions

Proton-gated singles spectra were recorded at 15, 16.5, 18, and 19.5 MeV projectile energies. A typical spectrum is shown in Fig. 1. These measurements served the dual functions of selecting the appropriate beam energy for subsequent experiments and providing spin information. The angular distribution and γ-γ coincidence experiments were run at 16.5 MeV. The primary reason for this choice was to minimize competition from ^{100}Mo(^{3}He,$3n\gamma$)^{100}Ru and reactions following the breakup of ^{3}He. ^{101}Mo γ rays from the $2p$ exit channel were included in the proton gated spectrum, but they were much weaker than the ^{101}Tc γ rays.

B. Angular distributions

The angular distribution measurement consisted of proton-gated singles spectra collected at 0°, 45°, and 90° with respect to the beam line. The angular distribution coefficients A_{kk}, were extracted using a least squares procedure and corrected for the detector solid angle. Particle and γ-ray emission reduces the original alignment of the com-

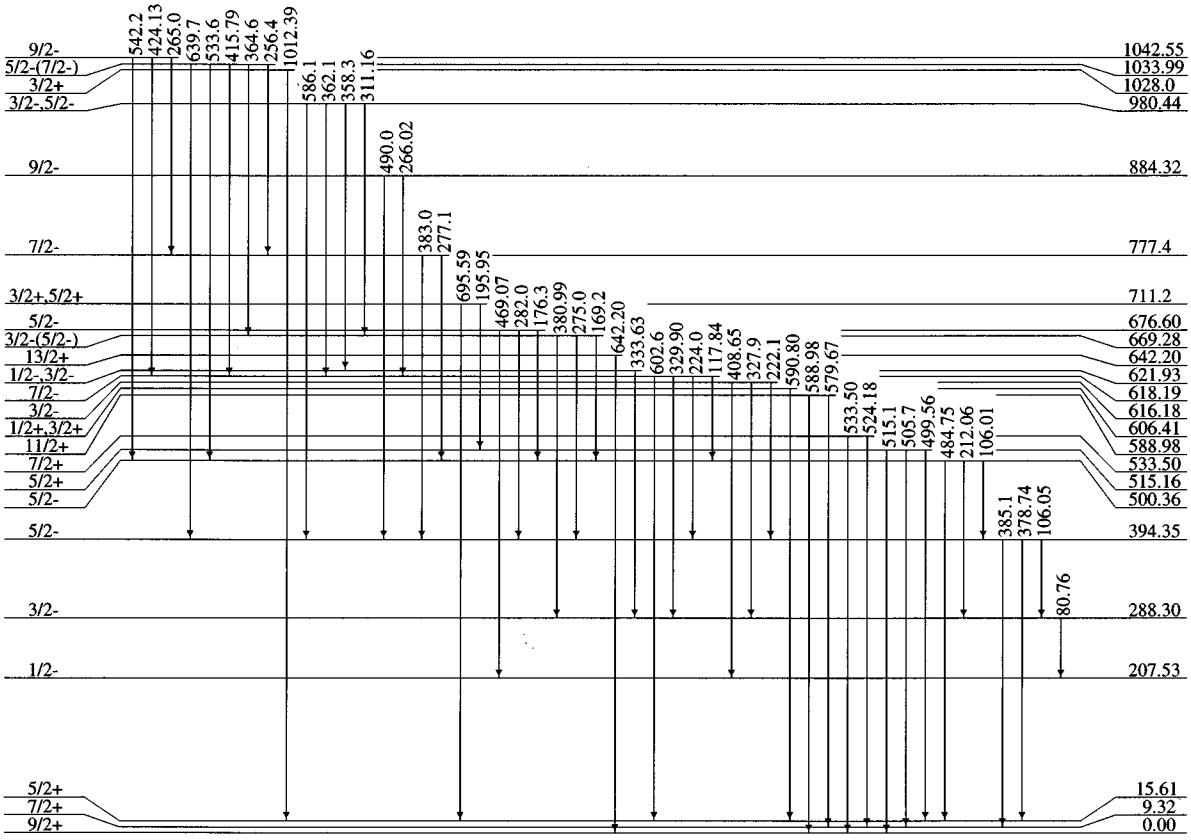

FIG. 2. The low-energy portion of the level scheme deduced for ^{101}Tc. Note that the vertcal energy scale is not linear.

pound system so that the experimental coefficients A_{kk} are smaller than the theoretical ones A_{kk}^0:

$$A_{kk} = \alpha_k A_{kk}^0 . \quad (1)$$

Typical values of α_k must be obtained from the experimental data using unmixed $E1$ and $E2$ transitions between states of known spin. Low-spin states are less orientated than high-spin states. α_2 varied in this experiment from approximately 0.2 for spin 5/2 to approximately 0.55 for spin 17/2. The α_4 is much smaller than α_2, hence the A_{44} coefficient usually was negligible for the orientations obtained in these experiments.

C. γ-γ coincidence measurement

The coincidence measurement was performed using two detectors positioned at 0° and 100° with respect to the beam axis. The data were stored as a 4096×4096 array in the computer memory. One-dimensional projections of the array also were accumulated (i.e., all γ rays in one detector that are in coincidence with any γ ray in the other detector). Coincidence peak areas, Compton ridges, and backgrounds were simultaneously determined by a three-dimensional least-squares fit [4] to the complete γ-γ coincidence matrix, rather than processing parts of the matrix condensed into one-dimensional gate spectra.

We rely on the coincidence results not only for yes-no criteria as to which γ transitions are in coincidence, but also for angular-momentum determinations and γ-ray intensities. Peak areas extracted in the fitting process were corrected for (1) γ-ray detector efficiency as a function of γ-ray energy, (2) γ-ray absorbtion in the chamber walls and detector windows, and (3) losses at low γ-ray energy caused by the timing circuits used with the γ-ray detectors.

III. THE LEVEL SCHEME

The level scheme deduced in the present work for ^{101}Tc is shown in Figs. 2 and 3. The low background in the proton-gated coincidence data allowed the placement of many weak transitions. 91 γ rays were identified as belonging to ^{101}Tc and placed unambiguously in the level scheme. The level scheme contains 49 states, 21 of which are new.

A tabular form of the level scheme is given in Table I. New states are marked with a superscript ''*a*'' following their energy. Most γ rays were placed by coincidence with γ rays that precede and follow in the decay pattern. In some cases several γ rays were assigned to the same state on the basis of energy agreement, because the observed feeding to the state was too weak to provide coincidence confirmation (indicated by a superscript ''*b*'' on the γ-ray energy). The precision of most γ-ray energy measurements was approximately 50 eV. Less accurate measurements are indicated by significant figures. The energy of the first three states was determined by γ rays that feed the states.

The spin and parity assignments are based on a combination of several sources: previous data compiled in Nuclear Data Sheets (NDS) [5,6], internal conversion measurements to determine the spins and parities of the low-lying states [7], two β-decay studies [8,9], a massive transfer study [10], a

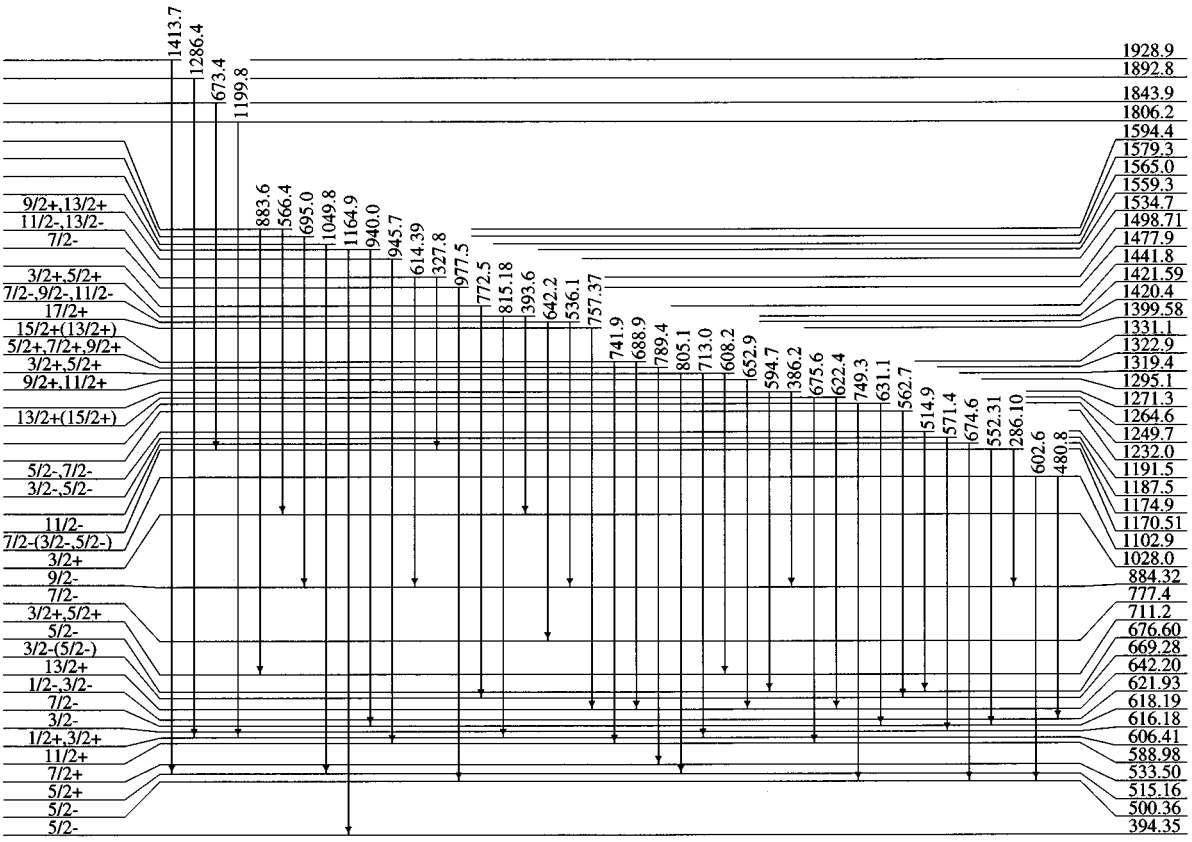

FIG. 3. The higher-energy portion of the level scheme deduced for ^{101}Tc. The energy scale is not linear.

proton stripping experiment [11], γ-ray branching patterns, and our analysis of excitation functions, angular distributions, and directional correlations in the coincidence data. Many new spin assignments were made and others were confirmed that had been considered tentative in NDS [5,6]. Ambiguity in spin assignment is indicated by multiple spin values. A tentative assignment is shown in parenthesis.

A γ-ray excitation function depends on the angular momentum of the state from which it is emitted. The excitation functions were normalized to that of the 212.06-keV transition from a $\frac{5}{2}^-$ state to remove the common energy dependence. Then the γ-ray intensity was fitted to an exponential function of energy:

$$I_\gamma \propto e^{bE}. \tag{2}$$

The exponential ''slope'' b is approximately proportional to the angular momentum of the state. (Variations of this technique are common [12,13].)

Equal slope intervals were used to estimate the angular momentum, as listed in Table II. These slope intervals were derived from transitions depopulating states of known spin [5,10]. A different set of intervals was necessary for positive- and negative-parity states. The ''data used'' column in Table I has an E when the excitation function was used to help assign angular momentum and parity to a state.

The angular distribution data were used to restrict angular momentum and parity choices. Only the general size and sign of the A_{22} was used because the degree of nuclear orientation was not well known. The measured A_{22} values are listed in Table I.

Additional angular momentum information was obtained from DCO analysis [14,15] of the coincidence data. (DCO stands for γ-γ directional correlation from oriented nuclei.) The DCO was used whenever there was substantial interference between γ rays or the uncertainty from the DCO was smaller than from the angular distribution. Complete DCO analysis [14] was performed but the DCO ratio was not given in Table I. Instead, we have calculated the value of A_{22} that the γ ray would have for the spin sequence and mixing ratio required by the experimental DCO ratio. Then the angular distribution and DCO measurements can be evaluated on the same basis. These ''implied'' A_{22} values are listed in Table I. The ''data-used'' column of Table I tells when the angular distribution (A) or DCO (D) was used in the spin analysis. A ''π'' subscript is added to A or D when the measurement does not allow parity change for the γ transition.

In general our spin assignments follow naturally from the information in Table I and the notations in the ''data used'' column. The assigned spin of the 288.30-keV level requires discussion. The proton stripping [11] and internal conversion [7] experiments limit the possible spin and parity to $1/2^-$ or $3/2^-$. The 212.06-keV transition from the $5/2^-$ 500.36-keV state, which feeds the 288.30-keV level, has a measured A_{22} value of 0.0 ± 0.03, which is inconsistent with a quadrupole transition unless the initial state is completely deoriented. Thus the assigned spin of the 288.30-keV state is $3/2^-$.

Our placement of three γ-ray transitions differs from that reported previously [10]. We did not observe a coincidence

TABLE I. Analysis of γ rays from ^{101}Tc.

E_i (keV)	I_i^π	E_γ (keV)	I_f^π	E_f (keV)	Intensities ^{101}Tc	Intensities Other	A_{22} × 100	Exc. func.	Data used [c]
9.32	$\frac{7}{2}^+$		$\frac{9}{2}^+$	0.00					N
15.60	$\frac{5}{2}^+$		$\frac{7}{2}^+$	9.32					N
			$\frac{9}{2}^+$	0.00					N
207.53	$\frac{1}{2}^-$		$\frac{5}{2}^+$	15.60					N
288.30	$\frac{3}{2}^-$	80.76	$\frac{1}{2}^-$	207.53	1000		−2(6)	112(14)	[11]
394.35	$\frac{5}{2}^-$	378.74	$\frac{5}{2}^+$	15.60	256		9(2)	2(3)	E,A [11]
		106.05	$\frac{3}{2}^-$	288.3	213	20	−4(5)	43(6)	
		385.1	$\frac{7}{2}^+$	9.32	35		−9(12)	27(28)	
500.36	$\frac{5}{2}^-$	212.06	$\frac{3}{2}^-$	288.3	352		0(3)	0(4)	E,A_π
		484.75	$\frac{5}{2}^+$	15.60	51		8(5)	26(13)	E,A
		106.01	$\frac{5}{2}^-$	394.35	20	213			
515.16	$\frac{5}{2}^+$	505.7	$\frac{7}{2}^+$	9.32	158	115			[11]
		499.56	$\frac{5}{2}^+$	15.60	35		13(4)	−30(11)	A
		515.1	$\frac{9}{2}^+$	0.00	22	28			
533.50	$\frac{7}{2}^+$	533.50	$\frac{9}{2}^+$	0.00	145	13	−6(2)	−29(4)	E,A_π
		524.18	$\frac{7}{2}^+$	9.32	56		−4(3)	−11(7)	A_π
588.98	$\frac{11}{2}^+$	588.98	$\frac{9}{2}^+$	0.00	163		26(3)	121(12)	E,A_π [10]
		579.67	$\frac{7}{2}^+$	9.32	39		18(5)	141(12)	E
606.41	$\frac{1}{2}^+$,$\frac{3}{2}^+$	590.80	$\frac{5}{2}^+$	15.60	180		0(3)	−121(10)	E, [8,9]
616.18	$\frac{3}{2}^-$	408.65	$\frac{1}{2}^-$	207.53	150		−5(3)	−71(3)	E,A
		327.9	$\frac{3}{2}^-$	288.3	28	6			
		222.1	$\frac{5}{2}^-$	394.35	8	11			
618.19	$\frac{7}{2}^-$	224.0	$\frac{5}{2}^-$	394.35	141	71	19(2)		D
		329.90	$\frac{3}{2}^-$	288.3	77		14(3)	51(10)	E,A,A_π
		117.84	$\frac{5}{2}^-$	500.36	45	10	−17(3)		D
		602.6	$\frac{5}{2}^+$	15.60	14	11			
621.93	$\frac{1}{2}^-$,$\frac{3}{2}^-$	333.63	$\frac{3}{2}^-$	288.3	105		−1(3)	−87(6)	E,A
642.20	$\frac{13}{2}^+$	642.20	$\frac{9}{2}^+$	0.00	200	8	24(3)	194(3)	E,A_π [10]
669.28	$\frac{3}{2}^-$($\frac{5}{2}^-$)	380.99	$\frac{3}{2}^-$	288.3	134		2(2)	−74(5)	E,A
		275.0	$\frac{5}{2}^-$	394.35	31	8			
		169.2	$\frac{5}{2}^-$	500.36	15	12			
676.60 [a]	$\frac{5}{2}^-$	469.07	$\frac{1}{2}^-$	207.53	137		11(3)	−25(3)	E,A,A_π
		282.0	$\frac{5}{2}^-$	394.35	24	6	15(5)		D,D_π
		176.3	$\frac{5}{2}^-$	500.36	18	10			
711.2	$\frac{3}{2}^+$,$\frac{5}{2}^+$	695.6	$\frac{5}{2}^+$	15.60	115	11	1(3)	−81(7)	E
		196.0	$\frac{5}{2}^+$	515.16	38	26			
777.4	$\frac{7}{2}^-$	277.1	$\frac{5}{2}^-$	500.36	57	10			
		383.0	$\frac{5}{2}^-$	394.35	35	17	−2(6)		D
884.32	$\frac{9}{2}^-$	490.0	$\frac{5}{2}^-$	394.35	71	34	19(5)		D_π
		266.02	$\frac{7}{2}^-$	618.19	62		14(5)	89(7)	E,A_π [10]
980.44 [a]	$\frac{3}{2}^-$,$\frac{5}{2}^-$	311.16	$\frac{3}{2}^-$($\frac{5}{2}^-$)	669.28	39		−12(8)	−31(10)	E,A
		358.3 [b]	$\frac{1}{2}^-$,$\frac{3}{2}^-$	621.93	9		−5(17)	243(54)	
		586.1 [b]	$\frac{5}{2}^-$	394.35	6	29			
		362.1 [b]	$\frac{7}{2}^-$	618.19	5	2			
1028.0	$\frac{3}{2}^+$	1012.4	$\frac{5}{2}^+$	15.60	96		−1(4)	−27(29)	N
1033.99 [a]	$\frac{5}{2}^-$($\frac{7}{2}^-$)	415.79	$\frac{7}{2}^-$	618.19	27		6(7)	0(17)	E,A_π

TABLE I. (*Continued*).

E_i (keV)	I_i^π	E_γ (keV)	I_f^π	E_f (keV)	Intensities ^{101}Tc	Intensities Other	A_{22} × 100	Exc. func.	Data used [c]
		639.7 [b]	$\frac{5}{2}^-$	394.35	16	8			
		364.6 [b]	$\frac{3}{2}^-(\frac{5}{2}^-)$	669.28	13		21(24)	8(23)	E
		533.6 [b]	$\frac{5}{2}^-$	500.36	12	146	−24(11)		D,D_π
		256.4 [b]	$\frac{7}{2}^-$	777.4	6	1			
1042.55 [a]	$\frac{9}{2}^-$	424.13	$\frac{7}{2}^-$	618.19	29		−24(4)	42(14)	A,A_π
		542.2 [b]	$\frac{5}{2}^-$	500.36	17		19(5)		D,D_π
		265.0 [b]	$\frac{7}{2}^-$	777.4	6	9			
1102.9	$\frac{7}{2}^-(\frac{3}{2}^-,\frac{5}{2}^-)$	602.6	$\frac{5}{2}^-$	500.36	8	17	−22(13)		D
		480.8 [b]	$\frac{1}{2}^-,\frac{3}{2}^-$	621.93	3	12			
1170.51	$\frac{11}{2}^-$	552.31	$\frac{7}{2}^-$	618.19	57		23(5)	130(17)	E,A_π [10]
		286.10	$\frac{9}{2}^-$	884.32	16		20(11)	191(17)	E
1174.9 [a]		674.6	$\frac{5}{2}^-$	500.36	5	36			
1187.54	$\frac{3}{2}^-,\frac{5}{2}^-$	571.4	$\frac{3}{2}^-$	616.18	19		7(12)	−74(35)	E
1191.5 [a]	$\frac{5}{2}^-,\frac{7}{2}^-$	514.9	$\frac{5}{2}^-$	676.6	28	22	−10(6)		D
1232.0 [a]		562.7	$\frac{3}{2}^-(\frac{5}{2}^-)$	669.28	5	4			
1249.7 [a]		749.3	$\frac{5}{2}^-$	500.36	6	6			
		631.1 [b]	$\frac{7}{2}^-$	618.19	5	3			
1264.6 [a]	$\frac{13}{2}^+(\frac{15}{2}^+)$	675.6	$\frac{11}{2}^+$	588.98	21	20			
		622.4 [b]	$\frac{13}{2}^+$	642.20	17		30(7)	200(22)	E,D,D_π
1271.3 [a]		594.7	$\frac{5}{2}^-$	676.6	31	100			
		386.2 [b]	$\frac{9}{2}^-$	884.32	7	10			
1295.1 [a]	$\frac{9}{2}^+,\frac{11}{2}^+$	652.9	$\frac{13}{2}^+$	642.20	16		3(11)	98(15)	E,D_π
1319.4	$\frac{3}{2}^+,\frac{5}{2}^+$	713.0	$\frac{3}{2}^+$	606.41	18		−9(16)	−148(20)	E,A
		805.1 [b]	$\frac{5}{2}^+$	515.16	8	25			
		608.2 [b]	$\frac{3}{2}^+,\frac{5}{2}^+$	711.2	7		−22(18)		A,A_π
1322.9 [a]	$\frac{5}{2}^+,\frac{7}{2}^+,\frac{9}{2}^+$	789.4	$\frac{7}{2}^+$	533.50	12	6			D,D_π
1331.1	$\frac{15}{2}^+(\frac{13}{2}^+)$	688.9	$\frac{13}{2}^+$	642.20	23		11(7)	234(23)	E,D_π [10]
		741.9 [b]	$\frac{11}{2}^+$	588.98	11	5			
1399.58	$\frac{17}{2}^+$	757.37	$\frac{13}{2}^+$	642.20	46		23(5)	275(9)	E,D_π [10]
1420.4 [a]	$\frac{7}{2}^-,\frac{9}{2}^-,\frac{11}{2}^-$	536.1	$\frac{9}{2}^-$	884.32	12	4	−15(13)		D,D_π
		642.2 [b]	$\frac{7}{2}^-$	777.4	8	200			
1421.59 [a]	$\frac{3}{2}^+,\frac{5}{2}^+$	815.18	$\frac{3}{2}^+$	606.41	37		−5(4)	−110(13)	E,A
		393.6 [b]	$\frac{3}{2}^+$	1028.0	9		11(17)	−89(27)	E
1441.8 [a]		772.5	$\frac{3}{2}^-(\frac{5}{2}^-)$	669.28	7	8			
1477.9 [a]	$\frac{7}{2}^-$	977.5	$\frac{5}{2}^-$	500.36	8	5	−35(17)		D,D_π
1498.71	$\frac{11}{2}^-,\frac{13}{2}^-$	614.39	$\frac{9}{2}^-$	884.32	20		24(5)	253(17)	E,D,D_π [10]
		327.8 [b]	$\frac{11}{2}^-$	1170.51	12	22	−14(10)		D
1521.1 [a]		844.5	$\frac{5}{2}^-$	676.6	5	14			
1534.7 [a]	$\frac{9}{2}^+,\frac{13}{2}^+$	945.7	$\frac{11}{2}^+$	588.98	7	30	−47(15)		D,D_π
1559.3 [a]		1164.9	$\frac{5}{2}^-$	394.35	6	10			
		940.0 [b]	$\frac{7}{2}^-$	618.19	4	72			
1565.0		1049.8	$\frac{5}{2}^+$	515.16	20	12			
1579.3 [a]		695.0	$\frac{9}{2}^-$	884.32	11	115			
1594.4		883.6	$\frac{3}{2}^+,\frac{5}{2}^+$	711.2	7	10			
		566.4 [b]	$\frac{3}{2}^+$	1028.0	4	12			

TABLE I. (*Continued*).

E_i (keV)	I_i^π	E_γ (keV)	I_f^π	E_f (keV)	Intensities ^{101}Tc	Intensities Other	A_{22} × 100	Exc. func.	Data used [c]
1806.2		1199.8	$\frac{3}{2}^+$	606.41	6	4			
1843.9 [a]		673.4	$\frac{11}{2}^-$	1170.51	15		13(16)		
1892.8		1286	$\frac{3}{2}^+$	606.41	6	17			
1928.9		1413.7	$\frac{5}{2}^+$	515.16	5	6			

[a]New states observed in this experiment.

[b]Placed in ^{101}Tc by coincidence with following γ rays, but assigned to this state on the basis of energy agreement.

[c]*N* means that the NDS [5,6] spin and parity assignment was used. *E*, *A*, or *D* means that the excitation function, angular distribution, or DCO, respectively, was used in the spin and parity assignment. A "π" subscript is added to *A* or *D* when the measurement excludes parity change for the γ transition.

between the 327.8- and 673.4-keV γ rays. We did observe coincidence cascades of 327.8-, 286.10-, and 266.02-keV γ rays, and of 673.4-, 286.10-, and 266.02-keV γ rays. Thus we have placed both the 327.8- and 673.4-keV transitions feeding the 1170.51-keV level, and the 552.31-keV transition depopulating the 1170.51-keV level.

IV. DISCUSSION AND INTERPRETATION

In recent years both IBFM [16] and rotational [2,4] models have been used to interpret collective structure in odd-*A* mass 100 nuclei. An IBFM calculation for the interpretation of ^{101}Tc was presented in previous work [10]. However, the authors found that the agreement was not satisfactory. There are clear signs that a rotational interpretation might be more promising. The level scheme of ^{101}Tc is marked by the $9/2^+$ ground state, and low-lying $7/2^+$, $5/2^+$, $1/2^-$, $3/2^-$, and $5/2^-$ states. The occurrences of these states at low excitation energies follow naturally if ^{101}Tc is deformed. The Nilsson [17] diagram appropriate for odd protons in ^{101}Tc is shown in Fig. 4. Since ^{101}Tc has 43 protons, the Fermi surface would lie near Nilsson states of spins $5/2^+$, $1/2^-$, $3/2^-$, and $5/2^-$ for deformations greater than $\delta = 0.15$. In the simplest Nilsson picture, the $7/2^+$ and $9/2^+$ members of a $5/2^+[422]$ rotational band would also lie at low excitation energies. When the Corioils interaction is included, states of these spins can be depressed in energy below the lowest $5/2^+$ state. In addition low-lying $1/2^+$ and $3/2^+$ states were observed at 606.41 keV and 711.19 keV. At deformations greater than $\delta = 0.18$, the $Z = 50$ shell closure disappears, and the $1/2^+[431]$ Nilsson state approaches the Fermi surface. A similar situation was found in ^{97}Tc [4], where a rotational calculation at a deformation of $\delta = 0.24$ successfully interpreted the observed structure. Since in the present work, the low-lying $7/2^+$ and $5/2^+$ states lie much closer to the ground state, and the $1/2^+$ and $3/2^+$ states lie $\sim$300 keV lower in excitation energy than in ^{97}Tc, the data indicate that ^{101}Tc is more deformed than ^{97}Tc. For these reasons the use of a rotational model at a higher deformation for the interpretation of the structure observed in ^{101}Tc seemed reasonable. A deformation of $\delta = 0.28$ gave the best results. In the comparison of the results of the calculation to the experimental results, emphasis has been placed on electromagnetic decay properties. Energies alone are not a sufficient basis for comparison, since frequently there are several states of the same spin and parity that have similar excitation energies. The comparison of experimental and calculated branching ratios provides a more reliable identification,

The rotational model used was a symmetric particle-plus rotor model. The calculation of energies and wave functions was the same as that used by Smith and Rickey [3] for Pd nuclei. The calculation of electromagnetic transition properties was the same as that used by Popli [18] for Ag nuclei. This specific model utilizes a rotational Hamiltonian in the strong-coupling limit, modified to include a variable moment of inertia (VMI) [19]. The basis states are thus rotational states built on Nilsson single-particle states [17], characterized by good K and Ω, the projections of the total angular momentum $\vec{I}$ and the particle angular momentum $\vec{j}$, respectively, on the symmetry axis. Pairing is treated by the BCS formalism. The Coriolis and recoil terms, which mix these states, are treated to all order. We would like to emphasize that this basic model has been used for years to interpret strongly deformed nuclei. Aside from differences in inertial quantities, the only deviations of its predictions from familiar rotational patterns are due to the role of the Coriolis interaction.

The predictions of the model fall between two extremes, which depend on the strength of the Coriolis interaction. When Coriolis mixing is small, the features of the basis,

TABLE II. Excitation function slope intervals for spin assignment.

	Slope interval			
	Positive parity		Negative parity	
Spin	Min.	Max.	Min.	Max
$\frac{1}{2}$		−190		−104
$\frac{3}{2}$	−190	−121	−104	−40
$\frac{5}{2}$	−121	−52	−40	+24
$\frac{7}{2}$	−52	+17	+24	+88
$\frac{9}{2}$	+17	+86	+88	+152
$\frac{11}{2}$	+86	+155	+152	+217
$\frac{13}{2}$	+155	+224	+217	
$\frac{15}{2}$	+224	+293		
$\frac{17}{2}$	+293			

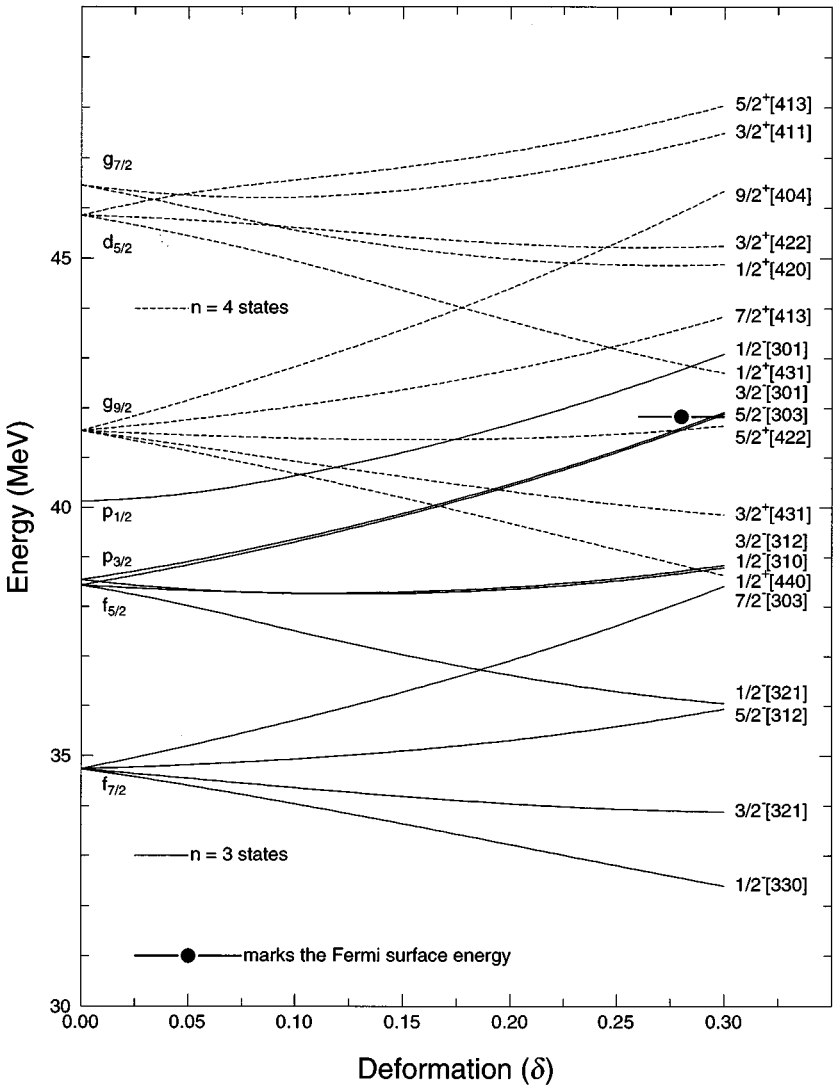

FIG. 4. Nilsson diagram for odd protons in ^{101}Tc.

namely rotational bands built on states of good Ω, are retained. This limit is approached not only when the deformation is high, but when low values of $\vec{j}$ are involved, or when $j \approx \Omega$. As Coriolis mixing increases, the odd particle tends to become decoupled from the rotating core. If the effects of the Coriolis interaction become large enough, the second limit is approached, in which R, the angular momentum of the core, and j are good quantum numbers rather than Ω. Thus the rotational predictions resemble particle-core multiplets rather than bands. This limit is most commonly realized in slightly deformed nuclei for states with a high, unique value of j. In ^{101}Tc, this might correspond to states of $g_{9/2}$ parentage. The determination of where observed states lie between these two limits is in effect a good assessment of the nuclear deformation.

The parameters used for the Nilsson calculations were

TABLE III. Parameters used in the calculation.

Shell number	κ	μ	μ_2	λ (MeV)	Δ (MeV)	Atten. factor
4	0.062	0.45	0.43	41.46	1.5	0.85
3	0.060	0.52	0.52	42.20	1.5	0.8

TABLE IV. Basis states and associated parameters used in the calculation.

State	E_{sp}	$\Im_0$	C
$\frac{1}{2}^+$ [420]	44.863	10.0	0.100
$\frac{1}{2}^+$ [431]	43.800	8.0	0.100
$\frac{1}{2}^+$ [440]	38.944	5.0	0.100
$\frac{3}{2}^+$ [411]	47.180	5.0	0.100
$\frac{3}{2}^+$ [422]	45.221	5.0	0.100
$\frac{3}{2}^+$ [431]	39.971	5.0	0.100
$\frac{5}{2}^+$ [413]	47.721	5.0	0.100
$\frac{5}{2}^+$ [422]	41.535	5.0	0.200
$\frac{7}{2}^+$ [413]	43.476	5.0	0.200
$\frac{9}{2}^+$ [404]	45.714	5.0	0.100
$\frac{1}{2}^-$ [301]	42.623	10.0	0.005
$\frac{1}{2}^-$ [310]	38.620	10.0	0.005
$\frac{1}{2}^-$ [321]	36.184	10.0	0.005
$\frac{3}{2}^-$ [301]	41.090	10.0	0.010
$\frac{3}{2}^-$ [312]	38.668	10.0	0.005
$\frac{5}{2}^-$ [303]	41.356	10.0	0.010

TABLE V. Comparison of experimental and calculated results for ^{101}Tc.

E_i							Theoretical identification	
Exp. (keV)	Theo. (keV)	I_i^π	I_f^π	E_γ (keV)	Branching ratio Exp.	Theo.	Initial state	Final state
0		$\frac{9}{2}+$					$g_{9/2}, R=0,2,4$	
9.32	−7	$\frac{7}{2}+$	$\frac{9}{2}+$				$g_{9/2}, R=2$	$g_{9/2}, R=0,2,4$
15.60	−14	$\frac{5}{2}+$	$\frac{7}{2}+$				$g_{9/2}, R=2,4$	$g_{9/2}, R=2$
			$\frac{9}{2}+$					$g_{9/2}, R=0,2,4$
207.53	207	$\frac{1}{2}-$	$\frac{5}{2}+$				$\frac{1}{2}^-[301]$	$g_{9/2}, R=2,4$
288.30	313	$\frac{3}{2}-$	$\frac{1}{2}-$	80.76	1.000	0.998	$\frac{1}{2}^-[301]$	$\frac{1}{2}^-[301]$
394.35	478	$\frac{5}{2}-$	$\frac{5}{2}+$	378.74	0.508	0.098	$\frac{1}{2}^-[301]$	$g_{9/2}, R=2,4$
			$\frac{3}{2}-$	106.05	0.423	0.900		$\frac{1}{2}^-[301]$
			$\frac{7}{2}+$	385.1	0.069	0.002		$g_{9/2}, R=2$
500.36	509	$\frac{5}{2}-$	$\frac{3}{2}-$	212.06	0.832	0.396	$\frac{5}{2}^-[303]$	$\frac{1}{2}^-[301]$
			$\frac{5}{2}+$	484.75	0.121	0.516		$g_{9/2}, R=2,4$
			$\frac{5}{2}-$	106.01	0.047	0.071		$\frac{1}{2}^-[301]$
515.16	700	$\frac{5}{2}+$	$\frac{7}{2}+$	505.7	0.735	0.684	$g_{9/2}, R=2,4,6$	$g_{9/2}, R=2$
			$\frac{5}{2}+$	499.56	0.163	0.310		$g_{9/2}, R=2,4$
			$\frac{9}{2}+$	515.1	0.102	0.006		$g_{9/2}, R=0,2,4$
588.98	478	$\frac{11}{2}+$	$\frac{9}{2}+$	588.98	0.807	0.737	$g_{9/2}, R=2,4$	$g_{9/2}, R=0,2,4$
			$\frac{7}{2}+$	579.67	0.193	0.263		$g_{9/2}, R=2$
606.41	687	$\frac{1}{2}+$ [b]	$\frac{5}{2}+$	590.80	0.950	0.050	$\frac{1}{2}^+[431]$	$g_{9/2}, R=2,4$
			$\frac{1}{2}-$	398.9 [d]	0.050	0.950		$\frac{1}{2}^-[301]$
616.18	591	$\frac{3}{2}-$	$\frac{1}{2}-$	408.65	0.806	0.609	$\frac{3}{2}^-[301]$	$\frac{1}{2}^-[301]$
			$\frac{3}{2}-$	327.92	0.151	0.355		$\frac{1}{2}^-[301]$
			$\frac{5}{2}-$	222.1	0.043	0.035		$\frac{1}{2}^-[301]$
618.19	683	$\frac{7}{2}-$	$\frac{5}{2}-$	224.0	0.509	0.842	$\frac{1}{2}^-[301]$	$\frac{1}{2}^-[301]$
			$\frac{3}{2}-$	329.90	0.278	0.149		$\frac{1}{2}^-[301]$
			$\frac{5}{2}-$	117.84	0.162	0.002		$\frac{5}{2}^-[303]$
			$\frac{5}{2}+$	602.6	0.051	0.000		$g_{9/2}, R=2,4$
642.20	632	$\frac{13}{2}+$	$\frac{9}{2}+$	642.20	1.000	0.996	$g_{9/2}, R=2$	$g_{9/2}, R=0,2,4$
669.28	779	$\frac{5}{2}-$ [b]	$\frac{3}{2}-$	380.99	0.744	0.624	$\frac{3}{2}^-[301]$	$\frac{1}{2}^-[301]$
			$\frac{5}{2}-$	275.0	0.172	0.369		$\frac{1}{2}^-[301]$
			$\frac{5}{2}-$	169.2	0.083	0.002		$\frac{5}{2}^-[303]$
711.2	692	$\frac{3}{2}+$ [b]	$\frac{5}{2}+$	695.6	0.752	0.518	$\frac{1}{2}^+[431]$	$g_{9/2}, R=2,4$
			$\frac{5}{2}+$	196.0	0.248	0.403		$g_{9/2}, R=2,4,6$
777.4	738	$\frac{7}{2}-$	$\frac{5}{2}-$	277.1	0.620	0.390	$\frac{5}{2}^-[303]$	$\frac{5}{2}^-[303]$
			$\frac{5}{2}-$	383.0	0.380	0.295		$\frac{1}{2}^-[301]$
			$\frac{7}{2}+$	768.1	0.000	0.111		$g_{9/2}, R=2$
884.32	932	$\frac{9}{2}-$	$\frac{5}{2}-$	490.0	0.534	0.570	$\frac{1}{2}^-[301]$	$\frac{1}{2}^-[301]$
			$\frac{7}{2}-$	266.02	0.466	0.424		$\frac{1}{2}^-[301]$
886 [a]	939	$\frac{5}{2}+$	$\frac{7}{2}+$	876.7	0.548	0.703	$\frac{1}{2}^+[431]$	$g_{9/2}, R=2$
			$\frac{5}{2}+$	870.4	0.452	0.220		$g_{9/2}, R=2,4$
1028.0	758	$\frac{3}{2}+$	$\frac{5}{2}+$	1012.4	1.000	0.838	$g_{9/2}, R=2,4$	$g_{9/2}, R=2,4$
			$\frac{5}{2}+$	512.8	0.000	0.104		$g_{9/2}, R=2,4,6$
1033.99	1025	$\frac{7}{2}-$ [b]	$\frac{7}{2}-$	415.79	0.365	0.340	$\frac{3}{2}^-[301]$	$\frac{1}{2}^-[301]$
			$\frac{5}{2}-$	639.7	0.216	0.513		$\frac{1}{2}^-[301]$
			$\frac{5}{2}-$	364.6	0.176	0.116		$\frac{3}{2}^-[301]$

TABLE V. (*Continued*).

E_i							Theoretical identification	
Exp. (keV)	Theo. (keV)	I_i^π	I_f^π	E_γ (keV)	Branching ratio Exp.	Theo.	Initial state	Final state
			$\frac{5}{2}^-$	533.6	0.162	0.016		$\frac{5}{2}^-[303]$
			$\frac{7}{2}^-$	256.4	0.081	0.003		$\frac{5}{2}^-[303]$
1042.55	1012	$\frac{9}{2}^-$	$\frac{7}{2}^-$	424.13	0.558	0.282	$\frac{5}{2}^-[303]$	$\frac{1}{2}^-[301]$
			$\frac{5}{2}^-$	542.2	0.327	0.540		$\frac{5}{2}^-[303]$
			$\frac{7}{2}^-$	264.95	0.115	0.070		$\frac{5}{2}^-[303]$
1170.51	1203	$\frac{11}{2}^-$	$\frac{7}{2}^-$	552.31	0.781	0.565	$\frac{1}{2}^-[301]$	$\frac{1}{2}^-[301]$
			$\frac{9}{2}^-$	286.1	0.219	0.430		$\frac{5}{2}^-[303]$
1249.66	1309	$[(\frac{9}{2}^-)]$ [c]	$\frac{5}{2}^-$	749.31	0.545	0.002	$\frac{3}{2}^-[301]$	$\frac{5}{2}^-[303]$
			$\frac{7}{2}^-$	631.12	0.455	0.603		$\frac{1}{2}^-[301]$
			$\frac{9}{2}^-$	365.4	0.000	0.271		$\frac{1}{2}^-[301]$
1295.1	1387	$\frac{11}{2}^+$ [b]	$\frac{13}{2}^+$	652.9	1.000	0.619	$g_{9/2}, R=2,4$	$g_{9/2}, R=2$
			$\frac{11}{2}^+$	706.1	0.000	0.255		$g_{9/2}, R=2,4$
1331.1	1330	$\frac{15}{2}^+$ [b]	$\frac{13}{2}^+$	688.89	0.676	0.485	$g_{9/2}, R=4$	$g_{9/2}, R=2$
			$\frac{11}{2}^+$	741.93	0.324	0.515		$g_{9/2}, R=2,4$
1399.58	1612	$\frac{17}{2}^+$	$\frac{13}{2}^+$	757.37	1.000	0.986	$g_{9/2}, R=4$	$g_{9/2}, R=2$
1420.4	1326	$\frac{11}{2}^-$ [b]	$\frac{9}{2}^-$	536.08	0.600	0.118	$\frac{5}{2}^-[303]$	$\frac{1}{2}^-[301]$
			$\frac{7}{2}^-$	642.2	0.400	0.696		$\frac{5}{2}^-[303]$
1498.71	1513	$\frac{13}{2}^-$ [b]	$\frac{9}{2}^-$	614.39	0.625	0.721	$\frac{1}{2}^-[301]$	$\frac{1}{2}^-[301]$
			$\frac{11}{2}^-$	327.78	0.375	0.280		$\frac{1}{2}^-[301]$
1534.7	1640	$\frac{13}{2}^+$ [b]	$\frac{11}{2}^+$	945.72	1.000	0.801	$g_{9/2}, R=4,6$	$g_{9/2}, R=2,4$
1579.29	1639	$[(\frac{11}{2}^-)]$ [c]	$\frac{9}{2}^-$	694.97	1.000	0.512	$\frac{3}{2}^-[301]$	$\frac{1}{2}^-[301]$
			$\frac{11}{2}^-$	408.8	0.000	0.293		$\frac{1}{2}^-[301]$
1843.93	1834	$[(\frac{15}{2}^-)]$ [c]	$\frac{11}{2}^-$	673.42	1.000	0.681	$\frac{1}{2}^-[301]$	$\frac{1}{2}^-[301]$
			$\frac{13}{2}^-$	345.2	0.000	0.319		$\frac{1}{2}^-[301]$

[a]State not observed in the present work. The energy and branching ratios are from [5].
[b]Other spins are allowed experimentally.
[c]The spin shown was not measured experimentally, but comes from the model association.
[d]Transition not observed in the present work. The relative intensity is from [5].

chosen to give energies at zero deformation consistent with those tabulated by Reehal and Sorenson [20]. The Fermi energies for positive and negative parities were chosen on the basis of filling Nilsson states with the 43 protons of ^{101}Tc, and then making minor adjustments. The pairing parameter Δ was taken from systematics. Coriolis and recoil terms were attenuated by the same factor. The values of these parameters are given in Table III.

The basis states for the calculation were restricted to the Nilsson states near the Fermi surface. The specific states included in the basis, along with their single-particle energies, are given in Table IV. In general we do not treat the VMI parameters $\mathfrak{I}_0$ and C as free parameters for all basis states, although different sets were adopted for positive- and negative-parity states. In the fine-tuning stage of the calculation, values were changed for four of the basis states. The VMI parameters are also given in Table IV.

Table V presents the comparison of experimental and calculated results for ^{101}Tc. This table includes only the experimental states that have been identified on the basis of their energies and branching ratios as corresponding to rotational states predicted by the model. Columns 1 and 2 give the experimental and theoretical energies for each initial state, and column 3 gives the initial spin and parity. If more than one spin was experimentally possible, only the spin agreeing with the theoretical spin is listed and identified with a footnote (there are nine states in this category). Three of the 31 initial states in this table had no experimental spin assignments, but are included because their energies and branching ratios agreed with those calculated. Values of I^π inferred from the model calculations are enclosed in double parentheses. The model identification of the initial state is given in column 8. In the calculation we considered decay probabilities to all final states to which transitions were possible on the basis of energies and spin changes. However, because of space limitations, the table only includes branches that were either observed or predicted to be observable. For the branches included, column 4 gives the final spin and parity and column 5 the γ-ray energy. Columns 6 and 7 give the experimental and theoretical branching ratios, and column 9

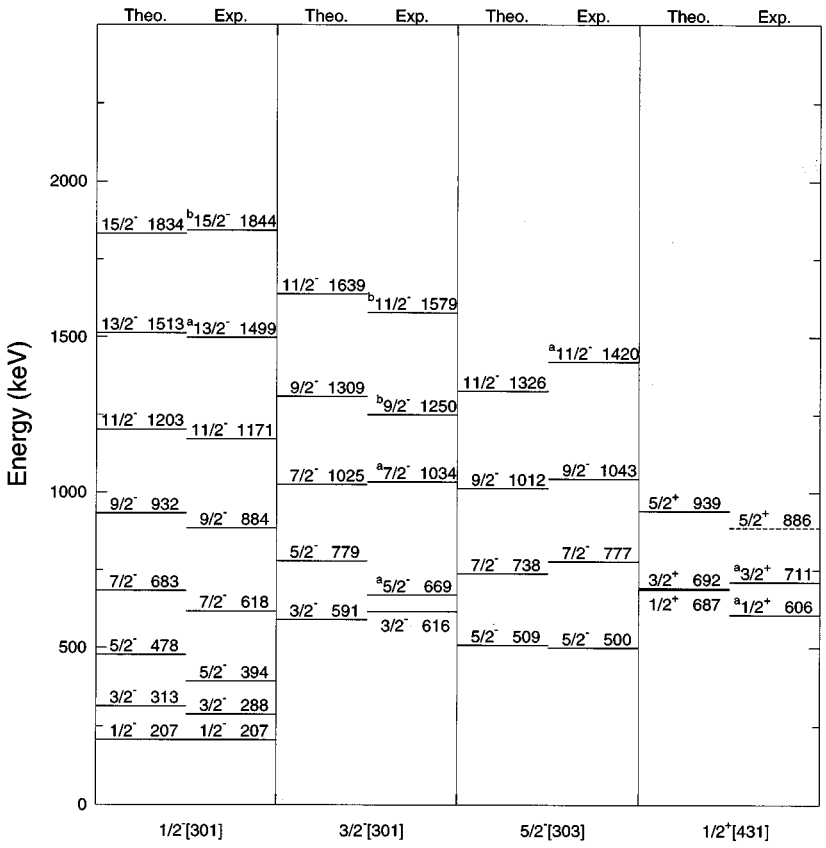

FIG. 5. Band structure identified in ^{101}Tc. The superscript ''a'' on an experimental spin indicates that the measurement allows for another spin. The superscript ''b'' indicates that no spin was measured, and that the spin shown is from the model association based on energy and branching ratios. The dashed state was not observed in the present work, and the energy and branching ratios are from Ref. [5].

gives the model identification for each final state.

Branching ratios played a major role in the inclusion or exclusion of experimental states in Table V. Consider the second $3/2^-$ state of the calculation, with a calculated energy of 591 keV. The calculation predicts the largest branch to the lowest $1/2^-$ state, with smaller branches to the lowest $3/2^-$ and $5/2^-$ states. Three candidates for this state on the basis of energy alone were observed experimentally, at 616.18, 621.93, and 669.28 keV. The latter two states have no observed branches to the lowest $1/2^-$ state. The 616.18-keV state decays as predicted, and hence is associated with the calculated state. The 669.28-keV state could also have spin-parity $5/2^-$. Another $5/2^-$ state was observed at 676.60 keV. Although the two states have similar energies, they have very different decay patterns. The third $5/2^-$ state of the calculation has a calculated energy of 779 keV, and the calculated decay agrees with the 669.28-keV experimental state. Thus this state is associated with the third $5/2^-$ state of the calculation, even though another spin is possible.

Three negative-parity ''bands'' have been identified, with bandheads $1/2^-$, $3/2^-$, and $5/2^-$. These three bands, along with the predicted energies, are shown in Fig. 5. Coriolis mixing is small because of the low values of j that contribute to the wave functions. The calculated wave functions for members of the $1/2^-$ band are better than 97% $1/2^-[301]$, so that the result is an essentially pure Nilsson band. The Coriolis interaction has caused some mixing for the $3/2^-$ and $5/2^-$ bands, although it is relatively small. Members of the $3/2^-$ band are better than 90% $3/2^-[301]$, and members of the $5/2^-$ band are better than 91% $5/2^-[303]$. Thus Table V identifies the bands as $1/2^-[301]$, $3/2^-[301]$, and $5/2^-[303]$, respectively.

In Table V three members of a positive-parity band with a bandhead spin of $1/2^+$ have also been identified. The calculation associates this band with a relatively pure $1/2^+[431]$ Nilsson band, ranging from 58% to 91% depending on the spin. This band, along with predicted energies, is also shown in Fig. 5. The fact that the bandhead decays at all by an $E1$ branch is a good indication of the $1/2^+[431]$ nature of the band. The model prediction of the $E1$ branch is much too large, but $E1$ calculations are extremely sensitive to small admixtures in the wave functions. The increase in Coriolis mixing over that for the negative-parity bands is due to components of higher values of j in the wave functions. However, the Coriolis mixing is still small enough so that no dominant j prevails.

The model associates the remaining positive-parity states included in Table V with Nilsson states of predominantly $g_{9/2}$ parentage. Although the Coriolis mixing is greater than for the bands discussed above, it is less than that observed in ^{97}Tc [4] and ^{99}Tc [21]. The energies of the lowest $9/2^+$, $7/2^+$, and $5/2^+$ states show this without examining the wave functions. In the basis, the order of these states in all three

TABLE VI. A comparison of the excitation energies of the three lowest positive-parity states in ^{97}Tc, ^{99}Tc, and ^{101}Tc.

	Excitation energy (keV)		
I^π	^{97}Tc	^{99}Tc	^{101}Tc
$\frac{9}{2}^+$	0.00	0.00	0.00
$\frac{7}{2}^+$	215.81	140.87	9.32
$\frac{5}{2}^+$	324.44	181.23	15.60

TABLE VII. Summary of calculated wave functions for states of predominantly $g_{9/2}$ parentage. Entries for Nilsson components, j, and R are fractions of total.

	Nilsson component					j	R			
Spin	[440]	[431]	[422]	[413]	[404]	(9/2)	0	2	4	6
$(\frac{1}{2})_2$	0.88					0.674	0.019	0.257	0.724	
$(\frac{3}{2})_2$	0.03	0.62				0.637	0.037	0.226	0.737	0.001
$(\frac{5}{2})_1$	0.08	0.31	0.61			0.906	0.069	0.666	0.265	
$(\frac{5}{2})_2$	0.41	0.23	0.33			0.710	0.085	0.299	0.511	0.106
$(\frac{7}{2})_1$	0.01	0.19	0.54	0.26		0.943	0.012	0.955	0.015	0.018
$(\frac{7}{2})_2$ [a]	0.06	0.28	0.02	0.45		0.666	0.070	0.224	0.696	0.002
$(\frac{9}{2})_1$	0.10	0.27	0.43	0.19	0.01	0.935	0.767	0.113	0.103	0.016
$(\frac{9}{2})_2$ [a]	0.32	0.21	0.04	0.38	0.04	0.919		0.530	0.437	0.021
$(\frac{11}{2})_1$	0.02	0.22	0.48	0.26	0.02	0.948		0.736	0.255	0.005
$(\frac{11}{2})_3$	0.07	0.38	0.01	0.42	0.11	0.929		0.130	0.396	0.497
$(\frac{13}{2})_1$	0.16	0.32	0.35	0.14	0.01	0.935		0.883	0.060	0.051
$(\frac{13}{2})_2$	0.32	0.12	0.10	0.37	0.06	0.948		0.004	0.761	0.215
$(\frac{15}{2})_1$	0.03	0.27	0.45	0.23	0.02	0.948			0.851	0.140
$(\frac{17}{2})_1$	0.23	0.37	0.28	0.10	0.01	0.936			0.912	0.060

[a]State not observed. The predicted decay is only to the lowest $\frac{5}{2}^+$ or $\frac{7}{2}^+$ state.

isotopes is $5/2^+$, $7/2^+$, and $9/2^+$. It is the Coriolis interaction that depresses the $9/2^+$ and $7/2^+$ states below the $5/2^+$ state. Table VI gives the experimental energies of these states in the three isotopes, and clearly the effects of the Coriolis interaction are smallest in ^{101}Tc, where the three states are essentially degenerate, in agreement with the calculation.

The calculated wave functions also show that Coriolis mixing is smaller, in that the results deviate more from the multiplet limit. Table VII gives a summary of the model wave functions. (Only the basis states of $g_{9/2}$ parentage are included. The fact that the Nilsson components do not total one for some states indicates components of other basis states.) It is clear that Ω is not a good quantum number. However, there is a trend for one Nilsson component to be larger than the others for many of the states. For example the lowest $5/2^+$, $7/2^+$, $9/2^+$, and $11/2^+$ states have a large $5/2^+[422]$ component, while the next states of spins $7/2^+$, $9/2^+$, and $11/2^+$ have a large $7/2^+[413]$ component. This is a shift towards ''bands'' (although subtle) compared to the wave functions obtained for ^{97}Tc [4]. The fraction of $j=9/2$ is high for all states in Table VII, but this is not an indication of the multiplet limit because the Nilsson states themselves are nearly pure $j=9/2$ states, ranging from 0.79 for the $1/2^+[440]$ state to 1.00 for the $9/2^+[404]$ state. Another sign of the smaller Coriolis mixing is that most of the wave functions contain more than one sizable value of R. Even the $9/2^+$ ground state, which should be a pure $R=0$ state in the multiplet limit, shows large components of $R=2$ and 4. In the identification column of Table V, more than one R component is listed if the dominant R component was less than 0.8.

There are of course observed states that are not described by this simple particle-rotor model. If one considers ^{100}Mo as the ''core'' for ^{101}Tc, there are five ''nonrotational'' excited states known [22] below 1.8 MeV, 0^+ (695 keV), 2^+ (1064 keV), 2^+ (1464 keV), 2^+ (1505 keV), and 4^+ (1870 keV). Thus one should expect to find ''nonrotational'' states in ^{101}Tc that are outside of the model space. Nevertheless, the model does a good job at low excitation energies. Of the 21 observed states below 1.0 MeV, 17 are accounted for by the model. As the excitation energy increases, there are more unexplained states. Between 1.0 and 1.5 MeV, 10 of the 22 observed states cannot be identified, and likewise for 6 of the 10 observed states between 1.5 and 2.0 MeV.

V. CONCLUSIONS

The present work has extended previously available information on the properties of intermediate-spin states in the low-energy region of ^{101}Tc. The ^{100}Mo(^{3}He,$pn\gamma$)^{101}Tc reaction has proven to be effective in populating both yrast and non-yrast states. 21 new levels have been established, which roughly doubles the number of known states below 2 MeV. The use of the proton-γ coincidence system, by reducing background and eliminating photopeaks from competing reaction channels, allowed the quantitative analysis of many weak transitions placed in the level scheme. As a result reliable spin assignments could be established for the majority of states.

The interpretation of the structure of ^{101}Tc in the framework of a rotational model has proven to be successful. Because of the larger deformation of ^{101}Tc ($\delta = 0.28$), the effects of the Coriolis interaction are smaller than in ^{97}Tc [4] and in ^{99}Tc [21].

Four reasonably pure rotational bands have been identified in ^{101}Tc, based on $1/2^-[301]$, $3/2^-[301]$, $5/2^-[303]$, and $1/2^+[431]$ Nilsson states. Coriolis mixing is smallest for the three negative-parity bands identified, and although somewhat larger in the positive-parity band identified, is still small enough to retain its nature as a $1/2^+[431]$ rotational band.

Positive-parity states for which $g_{9/2}$ parentage is deduced

exhibit a larger degree of Coriolis mixing. There is no consistent band structure for these states. However, many of the lowest-lying states have a large component of a single Nilsson state. For example, the lowest $5/2^+$ state is 61% $5/2^+[422]$. In addition this $5/2^+$ state lies at 15.60 keV, much lower than in ^{97}Tc or in ^{99}Tc. Both of these features point to a decrease in Coriolis mixing due to a larger deformation.

ACKNOWLEDGMENT

This work was supported in part by the National Science Foundation.

[1] C. S. Whistnant, K. D. Carnes, R. H. Castain, F. A. Rickey, G. S. Samudra, and P. C. Simms, Phys. Rev. C **34**, 443 (1986).
[2] Sadek Zeghib, F. A. Rickey, G. S. Samudra, P. C. Simms, and Ning Wang, Phys. Rev. C **36**, 939 (1987).
[3] H. A. Smith, Jr. and F. A. Rickey, Phys. Rev. C **14**, 1946 (1976).
[4] Hurol Aslan, Ben Crowe, Tim Dague, D. G. Savage, Sadek Zeghib, F. A. Rickey, and P. C. Simms, Phys. Rev. C **54**, 576 (1996).
[5] J. Blachot, Nucl. Data Sheets **45**, 701 (1985).
[6] J. Blachot, Nucl. Data Sheets **63**, 305 (1991).
[7] W. B. Cook, M. W. Johns, J. S. Geiger, and R. L. Graham, Can. J. Phys. **50**, 1511 (1972).
[8] W. B. Cook and M. W. Johns, Can. J. Phys. **50**, 1957 (1972).
[9] J. F. Wright, W. L. Talbot, and A. F. Voigt, Phys. Rev. C **12**, 572 (1975).
[10] H. Dejbakhsh, G. Mouchaty, and R. P. Schmitt, Phys. Rev. C **44**, 119 (1991).
[11] H. C. Cheung, J. Kitching, J. K. P. Lee, and S. K. Mark, J. Phys. G **7**, 737 (1975).
[12] W. Zipper, A. Dewald, W. Lieberz, R. Reinhardt, W. Dichter, F. Seiffert, and P. von Brentano, Nucl. Phys. **A504**, 36 (1989).
[13] Jean Kern, Pavel Cejnar, and Wiktor Zipper, Nucl. Phys. **A554**, 246 (1993).
[14] K. S. Krane, R. M. Steffen, and R. M. Wheeler, Nucl. Data, Sec. A **11**, 351 (1973).
[15] J. A. Grau, L. E. Samuelson, F. A. Rickey, P. C. Simms, and H. A. Smith, Phys. Rev. C **14**, 2297 (1976).
[16] *Interacting Bose-Fermion Systems in Nuclei*, edited by F. Iachello (Plenum, New York, 1981).
[17] S. G. Nilsson, K. Dan. Vidensk. Selsk. Mat. Fys. Medd. **29**, No. 16 (1955).
[18] Rakesh Popli, J. A. Grau, S. I. Popik, L. E. Samuelson, F. A. Rickey, and P. C. Simms, Phys. Rev. C **20**, 1350 (1979).
[19] M. A. J. Mariscotti, G. Scharff-Goldhaber, and B. Buck, Phys. Rev. **178**, 1864 (1969).
[20] B. Reehal and R. Sorenson, Phys. Rev. C **2**, 819 (1970).
[21] H.-W. Muller and D. Chemielewska, Nucl. Data Sheets **48**, 677 (1986).
[22] B. Singh and J. A. Szucs, Nucl. Data Sheets **60**, 1 (1990).